Spatiotemporal control of nanooptical excitations

Martin Aeschlimann[a], Michael Bauer[b], Daniela Bayer[a], Tobias Brixner[c], Stefan Cunovic[d], Frank Dimler[c], Alexander Fischer[a], Walter Pfeiffer[d,1], Martin Rohmer[a], Christian Schneider[a], Felix Steeb[a], Christian Strüber[d], and Dmitri V. Voronine[c]

[a]Fachbereich Physik and Research Center OPTIMAS, Technische Universität Kaiserslautern, Erwin-Schrödinger-Straße 46, 67663 Kaiserslautern, Germany; [b]Institut für Experimentelle und Angewandte Physik, Universität Kiel, Leibnizstraße. 19, 24118 Kiel, Germany; [c]Institut für Physikalische und Theoretische Chemie, Universität Würzburg, Am Hubland, 97074 Würzburg, Germany; and [d]Fakultät für Physik, Universität Bielefeld, Universitätsstrauße 25, 33615 Bielefeld, Germany

Edited* by Margaret M. Murnane, University of Colorado at Boulder, Boulder, CO, and approved February 1, 2010 (received for review November 23, 2009)

The most general investigation and exploitation of light-induced processes require simultaneous control over spatial and temporal properties of the electromagnetic field on a femtosecond time and nanometer length scale. Based on the combination of polarization pulse shaping and time-resolved two-photon photoemission electron microscopy, we demonstrate such control over nanoscale spatial and ultrafast temporal degrees of freedom of an electromagnetic excitation in the vicinity of a nanostructure. The time-resolved cross-correlation measurement of the local photoemission yield reveals the switching of the nanolocalized optical near-field distribution with a lateral resolution well below the diffraction limit and a temporal resolution on the femtosecond time scale. In addition, successful adaptive spatiotemporal control demonstrates the flexibility of the method. This flexible simultaneous control of temporal and spatial properties of nanophotonic excitations opens new possibilities to tailor and optimize the light–matter interaction in spectroscopic methods as well as in nanophotonic applications.

coherent control | nanophotonics | plasmonics | ultrafast spectroscopy

The interaction of light with matter is of fundamental importance in many areas of nature, science, and engineering, and the dynamics and efficiency of light-induced processes are determined by the properties of the optical field as a function of space and time at the location of interaction. Hence their most general investigation and exploitation would require the generation of light fields that can be specified at will in both their spatial and temporal degrees of freedom at all length and time scales. In the past, significant progress has been made toward realizing either of these two manipulation objectives separately. For temporal field properties, femtosecond laser pulse shaping (1) offers flexible control over the field amplitude, phase, and polarization (2, 3) on an ultrashort time scale. This has been exploited for coherent control over numerous quantum-mechanical systems (4, 5). For the case of spatial light-field properties, on the other hand, emerging nanooptical techniques (6) have made available spectroscopy beyond the Abbe diffraction limit, as, for example, nanoantenna-assisted addressing of individual molecules (7). Combination with femtosecond excitation offers high resolution in space and time (8–15) and opens routes toward novel applications (16, 17). In particular, deliberate spatial manipulation of optical near-field distributions was realized with adaptive and coherent control methods (9, 11–13, 18–22). In our recent demonstration of adaptive control of nanooptical fields (13), only spatial properties of optical near-field distributions were accessed. In the present work, in contrast, we directly measure and control also the temporal evolution of the nanoscale excitation. This information is obtained and exploited here using time-resolved cross-correlation measurements with one polarization-shaped "pump" light pulse and one bandwidth-limited "probe" pulse. The observed time-dependent cross-correlation patterns contain information on the local spatial excitation as well as the temporal evolution. We demonstrate the simultaneous control over spatial and temporal degrees of freedom of electromagnetic excitations in the vicinity of a nanostructure, and we achieve switching of the near-field localization with a lateral resolution well below the diffraction limit on a nanometer length scale and a temporal resolution on a few-femtosecond time scale.

Results

Fig. 1*A* shows the experimental scheme. The basic idea is that a suitable polarization-shaped (2, 3) femtosecond pump laser pulse creates a time- and space-dependent excitation pattern in a nanostructure—i.e., a transient spatial distribution of photoexcited electrons—that depends on the laser pulse shape, the local optical response of the nanostructure, and the coherent and inelastic lifetime of the electronic excitation in the material. The spatial excitation pattern is then monitored via time-resolved two-photon photoemission electron microscopy (23) using a circularly polarized probe pulse that excites the electrons from intermediate states into the continuum (Fig. 1*A*, *Inset*) as a function of a variable temporal delay τ. Note that the population of excited electrons dominates the time-resolved signal in the present case. Polarization pulse shaping (2, 3) is achieved by employing a zero-dispersion compressor and a two-layer 128-pixel LCD spatial light modulator in its Fourier plane. Intensity, phase, ellipticity, and orientation angle can thus be varied within a single pulse. Pulses are generated by a Ti:Sapphire oscillator at 75 MHz repetition rate, 795 nm center wavelength, and a bandwidth of about 25 nm. The pump pulse shown in Fig. 1*A* is created by splitting the spectrum in a red (>796 nm) and blue part (<796 nm), applying a phase difference of π between both LCD layers for the red part and identical linear spectral phases for the blue part. In addition, a linear spectral phase has been applied to separate the red and blue subpulses by 200 fs. The shaped pulses are characterized via dual-channel spectral interferometry using an independently determined reference pulse (2, 3). The much weaker bandwidth-limited probe pulse is circularly polarized to minimize the effect of a distinct polarization direction. It arrives at an adjustable delay τ (Fig. 1*A*) and in addition optical interference between pump and probe pulses is averaged out by a fast dither ($\pm$2 fs) of the temporal delay using a piezo-driven delay stage. Photoemission patterns (Fig. 1*C*–*E*) are recorded with better than 50-nm resolution by a photoemission electron microscope (PEEM) oriented along the z axis. After amplification with a microchannel plate, readout occurs either with a phosphorus screen and a Peltier-cooled CCD camera (for Fig. 1*C*) or a delay-line detector (24) (all other figures) that allows single-event counting and thus improves the detection of small

Author contributions: M.A., M.B., T.B., and W.P. designed research; D.B., S.C., F.D., A.F., M.R., C. Schneider, F.S., C. Strüber, and D.V.V. performed research; F.D., M.R., C. Schneider, F.S., C. Strüber, and D.V.V. analyzed data; and M.A., M.B., T.B., W.P., and C. Strüber wrote the paper.

The authors declare no conflict of interest.

*This Direct Submission article had a prearranged editor.

[1]To whom correspondence should be addressed. E-mail: pfeiffer@physik.uni-bielefeld.de.

This article contains supporting information online at www.pnas.org/cgi/content/full/0913556107/DCSupplemental.

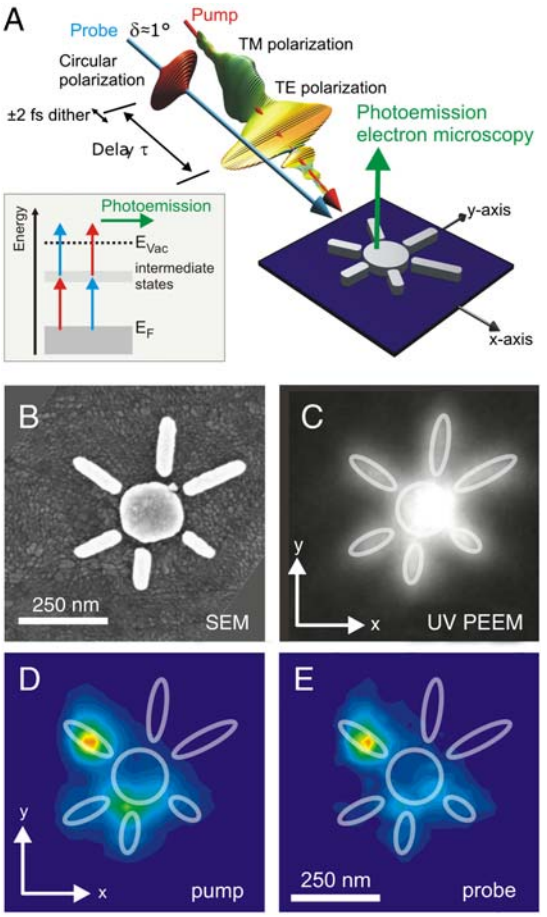

Fig. 1. (*A*) Experimental scheme. Polarization-shaped pump and circularly polarized probe laser pulses illuminate the surface (incidence angle of 65°, slightly different azimuth angles with difference angle δ) with adjustable time delay τ. The 3D pulse representations show amplitude envelopes of the electric field vector as a function of time, and the color indicates momentary frequency. The inset shows those two-photon excitation pathways for pump (red arrow) and probe interactions (blue arrow) that contribute to a τ-dependent signal and that promote electrons from below the Fermi level E_F via intermediate states to above the vacuum energy E_{vac}. (*B*) Scanning electron microscopy provides an image of an individual sun-shaped planar silver nanostructure. (*C*) One-photon-induced PEEM with UV light from a mercury vapor lamp shows emission from an individual nanostructure (gray outlines). (*D*–*E*) Normalized two-photon PEEM patterns are shown for excitation with the pump pulse (fluence 30 nJ cm^{-2}) only (*D*) and the probe pulse (fluence 3 nJ cm^{-2}) only (*E*), for pulse shapes as they are schematically represented in *A*.

signal variations. Long-term drifts within cross-correlation measurements are corrected by alternately recording PEEM patterns with and without pump excitation and using the latter as a position reference.

We investigate a "sun-shaped" planar silver nanostructure of 40-nm height on an indium tin oxide layer on glass (Fig. 1*B*). One-photon PEEM with ultraviolet light (Fig. 1*C*) reflects directly the geometry of the nanostructure and acts as a reference for time-resolved two-photon PEEM images. To facilitate two-photon photoemission around 795-nm wavelength, the surface was dosed with Cs to reduce the work function just below the two-photon photoemission threshold. Time-integrated two-photon PEEM patterns recorded with either the pump pulse only (Fig. 1*D*) or the probe pulse only (Fig. 1*E*) show very similar emission patterns. These signals form a time-independent background and therefore are measured separately and subtracted from the time-resolved PEEM patterns shown below.

In the first example of spatiotemporal control (Fig. 2), the polarization-shaped pump pulse as depicted in Fig. 1*A* is used to excite the nanostructure. The temporal amplitudes for the transverse electric (TE; black dashed line) and the transverse magnetic (TM; purple solid line) components are shown in Fig. 2*A*. After subtraction of the time-independent background generated by pump-only and probe-only two-photon photoemission this excitation leads to the time-dependent cross-correlation signal displayed in Fig. 2*B*. Pump and probe fluences are adjusted to 30 nJ cm^{-2} and 3 nJ cm^{-2}, respectively, to yield a strong pump-probe effect of about the same magnitude as the background emission. For the given fluences saturation effects in the two-photon photoemission process are excluded because the fraction of excited electrons remains below 10^{-3}, already taking into account that the local excitation might be enhanced by field localization effects. Apart from the total electron yield integrated over the whole nanostructure (black), we plot the individual signals from different spatial regions of interest (ROI 1 as dashed green and ROI 2 as solid red rectangle in Fig. 2*C* and *D*). The cross-correlation emission patterns for delay snapshots $\tau = 13$ fs (Fig. 2*C*) and $\tau = 213$ fs (Fig. 2*D*) display striking differences. For temporal overlap of the probe pulse with the first subcomponent of the polarization-shaped pump pulse (at $\tau = 13$ fs) the emission maximum is located in ROI 1 in the lower part of

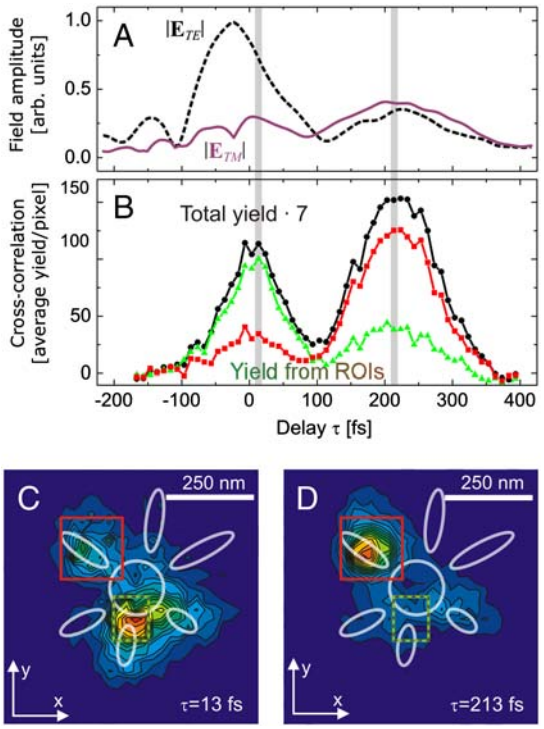

Fig. 2. Ultrafast switching of nanoscale excitation. (*A*) Time-dependent field amplitude for the TE (dashed black line) and TM (solid purple line) components of the polarization-shaped pump pulse that is also shown in 3D representation in Fig. 1*A*. The vertical gray bars indicate the delay for which cross-correlation patterns are shown in parts *C* and *D*. (*B*) Time-dependent cross-correlation signals are obtained after subtraction of the delay-time-independent background for the integrated photoemission yield from the whole nanostructure (black) and two different regions of interest (ROI 1 green dashed and ROI 2 solid red border) as defined in parts *C* and *D*. To facilitate the comparison the yield is displayed as average number of counts per CCD pixel. The curve representing the total emission is scaled by a factor of seven. (*C*–*D*) Normalized cross-correlation emission patterns after background subtraction are shown for the two different delays $\tau = 13$ fs (*C*) and $\tau = 213$ fs (*D*). The regions of interest for the time-dependent cross-correlation signals of *B* are indicated as solid red and dashed green rectangles in relation to the nanostructure (gray outlines).

the nanostructure (Fig. 2*C*), whereas it is located in ROI 2 for overlap with the second subcomponent (at $\tau = 213$ fs, Fig. 2*D*).

In Fig. 2*B*, local emission is switched with an "on–off" ratio of about three within a switching time that we set to 200 fs by design of the pump pulse. However, this is not the intrinsic switching speed limit of spatiotemporal control, which is rather determined by the bandwidth-limited pulse duration of about 40 fs. By reducing the temporal separation of the two subpulses of the pump pulse, we experimentally achieved spatial switching of the emission pattern with a switching time down to 50 fs. The switching time is limited by the lifetime of the collective plasmonic excitations of the nanostructure and by the lifetime of the photoexcited electrons in the intermediate states. In the present case, these two effects are negligible because the observed total cross-correlation signal (Fig. 2*B*, black line) closely follows the pump-pulse envelope and thus the involved lifetimes of collective and single-particle excitations must be short compared to the bandwidth limit of the pump pulse.

The regions of interest evaluated in Fig. 2*B* are separated by about 250 nm. The length scale over which local switching of excitations can be achieved is defined by the properties of the nanostructure that acts in the present case as an antenna for the incident radiation. Accordingly, ultrafast switching of nanosized patterns of photoexcited electrons is achieved with a spatial resolution below the $\lambda/2$ diffraction limit by exciting an individual nanostructure with a single polarization-shaped excitation pulse. The diffraction limit matters in the present context, because excitation switching on a larger scale could already be achieved by conventional far-field optics. Thus, it is the advantage of our concept to combine a suitably designed nanoantenna with femtosecond polarization shaping to overcome this far-field-optics limitation.

This demonstration of ultrafast nanoscale switching significantly differs from our previous work (13) in which time-integrated two-photon PEEM patterns were shifted in space only. Whereas this spatial control was achieved via the spatial field distribution and/or the field evolution in time, this ambiguity is overcome in the present investigation by the application of time-resolved two-photon photoemission measuring the cross-correlation of the excitation created by a polarization-shaped pump pulse and a bandwidth-limited probe pulse.

The choice of the particular pump-pulse shape of Fig. 1*A* was motivated by the expectation that two almost perpendicularly oriented subpulses lead to distinguishable excitation patterns, as it was indeed observed experimentally. Indeed, we have recently derived an analytic solution for the global optimum in spatial contrast control of nanostructure excitations (18). In that work we showed that, if a certain polarization pulse shape leads to optimal contrast between excitation at position A versus excitation at position B, then the opposite contrast (i.e., strong excitation at B and weak excitation at A) is achieved if the phase difference between the two excitation polarizations is changed by π. This is just what we have done in the example here: The phases applied to the two LCD layers differ by π for the red part of the spectrum and are identical for the blue part, i.e., the phase differences differ by π, and indeed the photoemission switches correspondingly between the two different regions of interest. In that sense, the excitation achieved with the sample pulse from Figs. 1*A* and 2 is an experimental confirmation of the analytic result (18). Still, besides the momentary polarization of the incident radiation, other control mechanisms, such as spectral switching and local spectral phase compensation (18, 19), might influence the spatiotemporal evolution of the excited-electron distribution. However, selective excitation of the two regions of the nanostructure by the different spectral distributions of the two subpulses of the pump pulse is excluded because each spectral component of the pump pulse shows the same spatial switching behavior if the polarization is changed from TM to TE. Hence we conclude that indeed the polarization degree of freedom is essential to achieve spatiotemporal control, as we have seen already in theoretical investigations (19). The localization of the excitations in either a gap region (TE polarization) or in one arm of the nanostructure (TM polarization) suggests that primarily the matching of the incident polarization to local excitation dipoles is the dominating control mechanism. It is important to note that this control mechanism does not rely on the interference of the coherences created by the two subpulses of the pump excitation.

The results presented up to now serve as a proof of principle for spatiotemporal control of local excitation. However, the method is more flexible because complex polarization-shaped laser pulses from closed-loop optimization can also be employed. Thus, one can realize complex space–time evolutions of excitation patterns. For this purpose, we use adaptive control in which the time-dependent PEEM signal is recorded with superimposed pump and probe pulses at one or several different delay positions τ serving as experimental feedback in a learning loop. An evolutionary algorithm (25) modifies the polarization pulse shape such that an electric near field with particular nanometer spatial *and* ultrafast temporal characteristics is created.

A demonstration example is shown in Fig. 3. Here the objective was again minimization and maximization of the emission ratio between two predefined regions of interest (solid red rectangle and sum of two dashed green rectangles in Fig. 3*C* and *D*) for two different time windows. Specifically, we desired excitation predominantly in the green region for $\tau = -500$ fs, and in the red region for $\tau = +500$ fs. To achieve this, the following strategy was pursued: The pump-pulse spectrum was divided in a long-

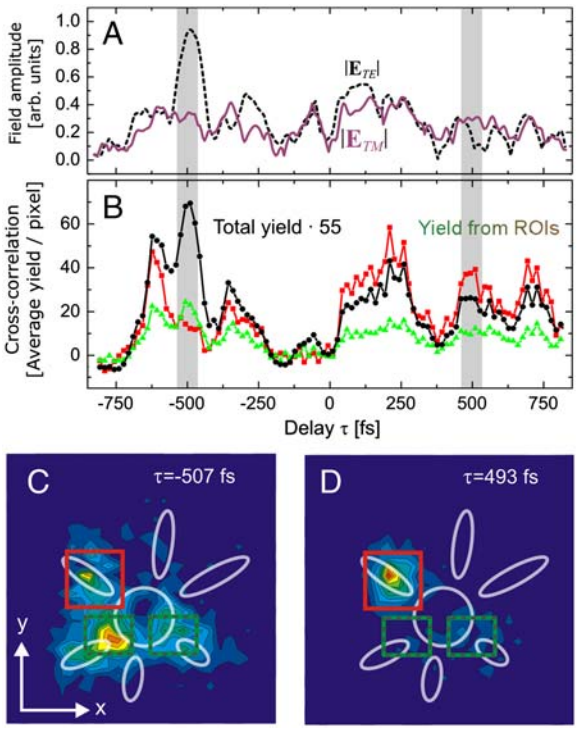

Fig. 3. Adaptive ultrafast spatiotemporal control. (*A*) The time-dependent field amplitude is shown for the TE (dashed black line) and TM (solid purple line) components of the adaptively optimized polarization-shaped pump pulse. Optimization time windows are indicated as gray-shaded bars. (*B*) Time-dependent cross-correlation signals after subtraction of the delay-independent background are shown for the total integrated photoemission yield (black, scaled by a factor of 55) and the two regions of interest (red and green). (*C*–*D*) Normalized cross-correlation emission patterns are shown after background subtraction for delays of $\tau = -507$ fs (*C*) and $\tau = 493$ fs (*D*), and the regions of interest are marked by colored rectangles.

wavelength (>796 nm) and a short-wavelength (<796 nm) part. Two independent optimizations were performed with superimposed pump and probe pulse at $\tau = 0$ fs, minimizing and maximizing the "red"/"green" emission ratio for the long- and short-wavelength part of the spectrum, respectively. The obtained optimized pulses were then shifted by 500 fs on the time axis by adding and subtracting linear spectral phases to the respective spectral regions, with the long-wavelength part shifted to earlier time. In the actual optimizations 10 free parameters, i.e., 10 phase values at different wavelength values, were used for each LCD layer. The 128 phase values for each layer were obtained from spline interpolation of the phase over the whole spectral range of the shaper. The maximum phase difference over the spectral range was limited to 20 rad. The spatial PEEM drift was determined from excitation patterns recorded with probe excitation only, directly before and after each generation. Each individual PEEM pattern from the corresponding generation was then corrected using the linearly interpolated momentary drift vector.

The envelopes of the resulting far-field TE and TM polarization components of the optimal pump pulse are shown in Fig. 3*A*, and the PEEM cross-correlation for the two regions in Fig. 3*B*. It is seen that indeed for the negative-time window the green curve is higher than the red one, and vice versa for the positive-time window. Temporal snapshots of the excitation pattern at $\tau = -507$ fs (Fig. 3*C*) and $\tau = 493$ fs (Fig. 3*D*) confirm the success of the optimization strategy with the desired spatiotemporal switching of emission.

The evolutionary algorithm explores a different strategy for reaching control than the one we adopted in the open-loop demonstration of Fig. 2. It can be seen that emission from the red region (Fig. 3*B*, red curve) is relatively high with respect to the total yield (black curve) throughout most of the pulse, only at the target window of $\tau = -500$ fs it is suppressed as desired. On the other hand, the time dependence of emission from the green region (green curve) follows closely the total emission (if scaled accordingly). But even so, the desired contrast to the red region is achieved. At first sight it might seem suspicious that the algorithm retrieves a complex field evolution (Fig. 3*A*) rather than one with reduced intensity outside of the gray bars. However, this simply reflects the fact that the feedback signal ("fitness") was defined for snapshots at two time positions only, and the other regions were not included, i.e., the PEEM signals at other times were not considered relevant. Thus the algorithm simply "moved" undesired excitation out of the temporal target window. The advantage of the adaptive approach, however, is that in a straightforward extension, one can use PEEM patterns for a larger number of different temporal delays between pump and probe as a feedback signal. Thus it will be possible to define complex time-dependent excitation patterns where the desired subwavelength spatial features can be specified at all time positions.

Discussion

The results shown up to now clearly demonstrate spatiotemporal control on a subwavelength length scale and a femtosecond time scale. However in the monitoring process, i.e., a two-photon photoemission process, both excitation pulses are involved and it is therefore important to disentangle the role of pump and probe pulse in the actually observed emission pattern. In the following we show that the observed cross-correlation signal indeed reflects the desired spatiotemporal control of a nanooptical excitation via polarization pulse shaping. Two observations indicate that primarily the pump pulse is responsible for the observed evolution of the PEEM pattern: (*i*) the total cross-correlation signal (Fig. 2*B*, black line) follows the envelope of the polarization-shaped pump pulse (Fig. 2*A*), and (*ii*) the probe excitation does not introduce an additional spatial preference of the total excitation since the time-integrated two-photon emission patterns for independent pump and probe excitation match closely (Fig. 1*D* and *E*). The strong emission contrast between Fig. 2*C* and *D* is therefore evidence that local excitation in the nanostructure is switched because of the time-dependent polarization of the pump pulse.

For rigorous analysis, one has to take into account (*i*) modification of the local field because of the collective electronic response of the nanostructure, (*ii*) interference of local fields generated by pump and probe pulse, (*iii*) superposition of two different two-photon excitation pathways (Fig. 1*A*, *Inset*), as well as (*iv*) electron relaxation and transport in the intermediate state. These effects are considered in the following theoretical derivation that starts with a space- and frequency-dependent response function (19) to obtain the local field for given external pump and probe pulse shapes. We consider parallel local transition dipole moments $\mathbf{p}_1(\mathbf{r})$ and $\mathbf{p}_2(\mathbf{r})$ for the first and second excitation steps, respectively, and we treat two-photon excitation and relaxation in the intermediate state with a rate model, i.e., under the assumption of instantaneous dephasing (26, 27). In polycrystalline silver films for electrons in intermediate states 1.5 eV above the Fermi energy, the energy relaxation lifetime is about 10 fs (28) and therefore cannot be resolved with the time resolution of about 40 fs in the experiment here. We show in *SI Text* that the cross-correlation PEEM signal using a time-dithered probe pulse is then given by

$$\begin{aligned} S(\mathbf{r},\tau) &= S^0(\mathbf{r}) + S^\tau(\mathbf{r},\tau) \\ &= p_1^2(\mathbf{r}) p_2^2(\mathbf{r}) \int_{-\infty}^{\infty} [I_\alpha^2(\mathbf{r},t) + I_\beta^2(\mathbf{r},t)]\,dt \\ &\quad + 4 p_1^2(\mathbf{r}) p_2^2(\mathbf{r}) \int_{-\infty}^{\infty} I_\alpha(\mathbf{r},t) I_\beta(\mathbf{r},t-\tau)\,dt\,. \end{aligned} \qquad [1]$$

Here $I_i(\mathbf{r},t)$ is the squared amplitude of the local electric field component that is parallel to the transition dipole moments $\mathbf{p}_1(\mathbf{r})$ and $\mathbf{p}_2(\mathbf{r})$ and that is generated by illumination with the pump pulse ($i = \alpha$) or the probe pulse ($i = \beta$). The first term, $S^0(\mathbf{r})$, describes the time-independent background from pump pulse and probe pulse alone (Fig. 1*D* and *E*) that is subtracted in the experimental results (Fig. 2*C* and 2*D*). From the second term, $S^\tau(\mathbf{r},\tau)$, it is evident that the background-free local photoemission yield can indeed be interpreted as cross-correlation between the local excitations generated by the local optical fields related to pump (α) and probe pulses (β), respectively. Note that the local excitations are pure populations because instantaneous dephasing is assumed in the present case. Because the probe pulse is bandwidth-limited (i.e., unshaped and roughly Gaussian) and because the probe pulse does not introduce a spatial emission preference in comparison to the time-integrated emission pattern of the pump pulse alone (Fig. 1*D* and *E*), any variation of the observed cross-correlation must be attributed to the effect of the shaped pump pulse. In other words, Eq. **1** proves that, because $I_\beta(\mathbf{r},t)$ is unshaped, any spatiotemporal evolution $S^\tau(\mathbf{r},\tau)$ of the PEEM patterns observed experimentally must arise from an ultrafast space-time variation $I_\alpha(\mathbf{r},t)$ of the excitation due to the polarization-shaped pump pulse. What is then the control mechanism? The local field amplitude $\sqrt{I_\alpha(\mathbf{r},t)}$ arises either from constructive or destructive interference of two different near-field modes excited by the two far-field TE/TM components or from the matching of the incident polarization to local dipoles (19). In both cases, the spatial excitation pattern is determined by the polarization shape and the desired time structure of the local excitation is controlled by the correct spectral phase (19).

The nanostructure and its spectral response play an important role in the achieved control. The nanostructure is designed to facilitate the anticipated control mechanisms (18, 19) and was chosen to exhibit significant symmetry breaking (different arm lengths), polarization sensitivity (orientation of the arms), and a chance that different localized modes interfere in the center

dot of the "sun." One of our target areas for switching was located in the gap region between an arm and the center dot. In case of TE excitation, the gap mode of the particular arm and the center dot is responsible for the localized excitation. This mode has a dipole moment oriented along the arm and should strongly couple to TE polarized light because the arm is oriented along the *y* direction. In contrast, the other of the two target areas was located close to the center of one arm. This area is more strongly excited with TM-polarized illumination because the arm is oriented almost in *x* direction. A strong interference of near-field modes is anticipated in the center dot of the nanostructure and there no significant spatial switching is apparent. Therefore the dominant control mechanism in the present case is the matching of the incident polarization to localized plasmonic modes of the particular nanostructure.

Summarizing, we have demonstrated spatiotemporal control of optical near-field distributions via the excitation with polarization-shaped light pulses. The theoretical treatment shows that the time-resolved two-photon photoemission cross-correlation signal indeed directly reflects the evolution of the local excitation in a nanostructure. In the limit of fast dephasing and short excited-electron lifetime the local excitation of electrons reflects the fields at the surface and thus maps also the local optical near-field evolution. Spatiotemporal excitation control as demonstrated experimentally in this work opens fascinating possibilities for studying electronic relaxation and transport within nanostructures, as pump and probe interactions can be separated both temporally and spatially on the relevant time and length scales. An even broader range of applications is conceivable if the nanostructure is used as a tailored antenna for a system located in its vicinity. For example, one could study electronic couplings and transport with direct spatiotemporal resolution in molecular assemblies, coupled quantum dots, nanowires, or similar systems. From the perspective of coherent control, the method provides nanoscale space–time manipulation beyond the dipole approximation: Extended quantum wave functions would experience a complex spatially inhomogeneous time-dependent excitation such that in comparison to plane-wave excitation many more degrees of freedom are available. Thus light–matter interaction could be optimized in a very general way for usage in many branches of fundamental and applied research such as for novel spectroscopic and microscopic methods, nanosensing, optical information processing, or quantum computation.

ACKNOWLEDGMENTS. We thank the Nano-Bio Center at the University of Kaiserslautern for support in the preparation of the nanostructures. This work was supported by the German Science Foundation within the SPP 1391 (to M.A., M.B., T.B., W.P.), the GRK 792 (to F.S.), the GRK 1221, the Emmy Noether Program (T.B.), and the SFB 677 (M.B.).

1. Weiner AM (2000) Femtosecond pulse shaping using spatial light modulators. *Rev Sci Instrum* 71:1929–1960.
2. Brixner T, Gerber G (2001) Femtosecond polarization pulse shaping. *Opt Lett* 26:557–559.
3. Brixner T, Krampert G, Niklaus P, Gerber G (2002) Generation and characterization of polarization-shaped femtosecond laser pulses. *Appl Phys B: Lasers Opt* 74:s133–s144.
4. Rice SA, Zhao M (2000) *Optical Control of Molecular Dynamics* (Wiley Interscience, New York), pp 39–240.
5. Brumer PW, Shapiro M (2003) *Principles of the Quantum Control of Molecular Processes* (Wiley, New York), pp 117–321.
6. Novotny L, Hecht B (2006) *Principles of Nano-Optics* (Cambridge Univ Press, Cambridge), pp 134–224.
7. Taminiau TH, Stefani FD, Segerink FB, van Hulst NF (2008) Optical antennas direct single-molecule emission. *Nat Photonics* 2:234–237.
8. Sanchez EJ, Novotny L, Xie XS (1999) Near-field fluorescence microscopy based on two-photon excitation with metal tips. *Phys Rev Lett* 82(20):4014–4017.
9. Stockman MI, Faleev SV, Bergman DJ (2002) Coherent control of femtosecond energy localization in nanosystems. *Phys Rev Lett* 88:067402.1–067402.4.
10. Stockman MI (2004) Nanofocusing of optical energy in tapered plasmonic waveguides. *Phys Rev Lett* 93:137404.1–137404.4.
11. Brixner T, García de Abajo FJ, Schneider J, Pfeiffer W (2005) Nanoscopic ultrafast space-time-resolved spectroscopy. *Phys Rev Lett* 95:093901.1–093901.4.
12. Kubo A, et al. (2005) Femtosecond imaging of surface plasmon dynamics in a nanostructured silver film. *Nano Lett* 5:1123–1127.
13. Aeschlimann M, et al. (2007) Adaptive subwavelength control of nanooptical fields. *Nature* 446:301–304.
14. Ropers C, Solli DR, Schulz CP, Lienau C, Elsaesser T (2007) Localized multiphoton emission of femtosecond electron pulses from metal nanotips. *Phys Rev Lett* 98:043907.1–043907.4.
15. Durach M, Rusina A, Stockman MI, Nelson KA (2007) Toward full spatiotemporal control on the nanoscale. *Nano Lett* 7:3145–3149.
16. Kim S, et al. (2008) High-harmonic generation by resonant plasmon field enhancement. *Nature* 453:757–768.
17. MacDonald KF, Samson ZL, Stockman MI, Zheludev NI (2009) Ultrafast active plasmonics. *Nat Photonics* 3:55–58.
18. Tuchscherer P, et al. (2009) Analytic control of plasmon propagation in nanostructures. *Opt Express* 17:14235–14259.
19. Brixner T, García de Abajo FJ, Schneider J, Spindler C, Pfeiffer W (2006) Ultrafast adaptive optical near-field control. *Phys Rev B: Condens Matter Mater Phys* 73:125437.1–125437.11.
20. Sukharev M, Seideman T (2006) Phase and polarization control as a route to plasmonic nanodevices. *Nano Lett* 6:715–719.
21. Stockman MI, Kling MF, Kleineberg U, Krausz F (2007) Attosecond nanoplasmonic-field microscope. *Nat Photonics* 1:539–544.
22. Li XT, Stockman MI (2008) Highly efficient spatiotemporal coherent control in nanoplasmonics on a nanometer-femtosecond scale by time reversal. *Phys Rev B: Condens Matter Mater Phys* 77:195109.1–195109.10.
23. Schmidt O, et al. (2002) Time-resolved two photon photoemission electron microscopy. *Appl Phys B: Lasers Opt* 74:223–227.
24. Oelsner A, Krasyuk A, Nepijko S, Schneider CM, Schönhense G (2005) Spatially resolved observation of dynamics in electrical and magnetic field distributions by means of a delayline detector and PEEM. *J Electron Spectrosc Relat Phenom* 144:147–776.
25. Baumert T, Brixner T, Seyfried V, Strehle M, Gerber G (1997) Femtosecond pulse shaping by an evolutionary algorithm with feedback. *Appl Phys B: Lasers Opt* 65:779–782.
26. Weida MJ, Ogawa K, Nagano H, Petek H (2000) Ultrafast interferometric pump-probe correlation measurements in systems with broadened bands or continua. *J Opt Soc Am B* 17:1443–1451.
27. Merschdorf M, Kennerknecht C, Pfeiffer W (2004) Collective and single-particle dynamics in time-resolved two-photon photoemission. *Phys Rev B: Condens Matter Mater Phys* 70:193401.1–193401.4.
28. Aeschlimann M, et al. (2000) Transport and dynamics of optically excited electrons in metals. *Appl Phys A: Mater Sci Process* 71:485–491.